

Article

Comparative Study of Indoor Propagation Model Below and Above 6 GHz for 5G Wireless Networks

Ahmed Mohammed Al-Samman ^{1,*}, Tharek Abd. Rahman ¹, Tawfik Al-Hadhrani ^{2,*}, Abdulalama Daho ¹, MHD Nour Hindia ³, Marwan Hadri Azmi ¹, Kaharudin Dimiyati ³ and Mamoun Alazab ⁴

¹ Wireless Communication Centre, Faculty of Engineering, Universiti Teknologi Malaysia, Johor Bahru 81310, Malaysia; tharek@fke.utm.my (T.A.R.); abdulalamautm2017@gmail.com (A.D.); hadri@fke.utm.my (M.H.A.)

² School of Science and Technology, Nottingham Trent University, Nottingham NG11 8NS, UK

³ Department of Electrical Engineering, Faculty of Engineering, University of Malaya, Kuala Lumpur 50603, Malaysia; nourhindia@hotmail.com (M.N.H.); kaharudin@um.edu.my (K.D.)

⁴ College of Engineering, IT and Environment, Charles Darwin University, Darwin 0815, Australia; Alazab.m@ieee.org

* Correspondence: ahmedsecure99@gmail.com (A.M.A.-S.); Tawfik.al-hadhrani@ntu.ac.uk (T.A.-H.); Tel.: +44-115-848-4818 (T.A.-H.)

Received: 30 November 2018; Accepted: 26 December 2018; Published: 1 January 2019



Abstract: It has been widely speculated that the performance of the next generation based wireless network should meet a transmission speed on the order of 1000 times more than the current cellular communication systems. The frequency bands above 6 GHz have received significant attention lately as a prospective band for next generation 5G systems. The propagation characteristics for 5G networks need to be fully understood for the 5G system design. This paper presents the channel propagation characteristics for a 5G system in line of sight (LOS) and non-LOS (NLOS) scenarios. The diffraction loss (DL) and frequency drop (FD) are investigated based on collected measurement data. Indoor measurement results obtained using a high-resolution channel sounder equipped with directional horn antennas at 3.5 GHz and 28 GHz as a comparative study of the two bands below and above 6 GHz. The parameters for path loss using different path loss models of single and multi-frequencies have been estimated. The excess delay, root mean square (RMS) delay spread and the power delay profile of received paths are analyzed. The results of the path loss models show that the path loss exponent (PLE) in this indoor environment is less than the free space path loss exponent for LOS scenario at both frequencies. Moreover, the PLE is not frequency dependent. The 3GPP path loss models for single and multi-frequency in LOS scenarios have good performance in terms of PLE that is as reliable as the physically-based models. Based on the proposed models, the diffraction loss at 28 GHz is approximately twice the diffraction loss at 3.5 GHz. The findings of the power delay profile and RMS delay spread indicate that these parameters are comparable for frequency bands below and above 6 GHz.

Keywords: 5G; smart city; IoT; channel propagation; 3.5 GHz; 28 GHz; delay spread; path loss

1. Introduction

Enabling consumers to do all the things they do today with mobile devices (such as smartphones and tablets) faster and more reliably, 5G may support new ways of using those mobile devices (e.g., new applications), and completely new types of mobile devices [1,2]. As the number of mobile users increases, 5G communication networks/base stations must handle a greater amount of data and move toward considerably higher speeds than those of the base stations that make up today's cellular networks [3,4].

5G networks are also envisaged to use resource sharing for both heavily bandwidth thirsty video applications and for handling data traffic from large cluster of sensors i.e., the so-called Internet of Things (IOT) [5,6]. The new IoT applications are enabling smart city initiatives worldwide [7]. Using IOT applications, the mobile users are able to monitor and control devices with high stream of real-time information. IoT requires huge amount of bandwidth, which is needed to support massive sensors [8,9].

IoT based smart cities have various real-time applications which would be crucial and useful for the next generation of network [10]. The application can be classified into two major group i.e., smart energy and smart transportation [5].

Therefore, the main problem for current wireless networks is that a huge amount of data will be required more than before, which will be congested on the radio-frequency spectrum below 6 GHz. This implies that slower service and more dropped connections occur due to the low bandwidth. Therefore, the millimeter wave (mm-wave) band is chosen as a potential candidate for the next generation wireless networks, i.e., 5G, where more bandwidths are available with up to 10 times the capacity of today's cellular networks [11]. Moreover, the feasibility of mobile broadband systems in frequency bands above 6 GHz has been reported in academic and industry research [1,12–15]. For frequency bands below 6 GHz, it is worth to note that the licensed spectrum of 3.5 GHz could be potentially allocated for 5G applications [4,16]. Various studies have been done which explains that the 3.5 GHz frequency band work as main access link for indoor communication whereas, the 28 GHz can be used as a backhaul link [4,17,18].

In this context, this paper investigates the diffraction loss (DL) and frequency drop (FD) based on comparative study for indoor propagation channel characteristics at 3.5 GHz and 28 GHz bands. DL is used to calculate the amount of loss due to the diffraction from wall edge in indoor environment. FD is used to estimate the signal degradation when the frequency is high (above 6 GHz) based on comparison with the received signal at lower band (below 6 GHz). The contributions of this paper can be defined in four folds as follows.

- Firstly, the propagation characteristics for the 5G channel at frequencies of 3.5 GHz and 28 GHz are compared in an indoor environment. The line of sight (LOS) and non-LOS (NLOS) measurements were performed using the ultra-wideband correlation channel sounder with a higher chip rate of 1000 Megachips-per-second (Mcps) as well as a higher resolution of 1 ns.
- Secondly, two physically based models; the close-in (CI) free space reference and the CI model with a frequency-weighted path loss exponent (CIF) are used to investigate the single and multi-frequency statistical path loss, respectively. Two 3GPP path loss models; floating intercept (FI) and alpha-beta-gamma (ABG) models are also used to investigate the propagation characteristic for a single and multi-frequency statistical models, respectively.
- Thirdly, DL and FD are used to analyze the signal degradation due to the shadow edge effect and high operating frequency.
- In the last, the power delay profile, root mean square (RMS) delay spread and mean excess (MN-EX) delay, are considered to characterize the time dispersion parameters for both frequency bands.

The remainder of this paper is organized as follows. Related work has been described in Section 2. The proposed path-loss models are presented in Section 3, with time dispersion parameters are proposed in Section 4. Section 5 describes the experimental setup. The results are discussed in Section 6, while Section 7 summarizes the findings of the study as conclusions.

2. Related Work

Mm-wave communications have recently attracted large research interest, since the huge available bandwidth can potentially lead to the rates of multiple gigabit per second per user [19]. The industry often uses the term mm-wave to define frequencies between 10 GHz and 300 GHz [20]. The wavelengths

of mm-wave frequencies ranges from 1 mm to 100 mm compared to the radio waves that serve today's devices, which measure wavelengths in the order of tens of centimeters.

In the past, the mm-wave spectrum has been proposed for wireless local area networks (WLANs), intelligent transport systems (ITS's), personal communication network (PCN) systems and local multipoint distribution systems (LMDS) [21]. It has also been used in satellite communications, long-range point-to-point communications and military applications [20]. Currently, some cellular providers use mm-wave frequencies for data transmission between stationary points, such as two base stations [20]. However, using them to connect the base station with mobile terminals is an entirely different approach. The amount of available bandwidth in mm-wave bands including frequencies above 6 GHz i.e., the 28 GHz band help in the deployment of 5G. The future 5G wireless networks require a huge capacity to connect anything-anywhere at any time. With mm-wave bands, massive multiple-input multiple-output (MIMO) and other 5G technologies, the wireless network will be able to serve the future smartphone users, robotics [22], remote surgeries [23], and autonomous cars [24,25]. Already, elevated expectations have been set for 5G by promising ultralow latency and record-breaking data speeds for consumers. However, there are some challenges for 5G wireless network, such as difficult propagation conditions using high frequency i.e., 28 GHz band [26]. These propagation difficulties can be countered by using multiple highly directional antennas [27]. The very short transmission time interval (TTI) that characterizes the mm-wave makes it very much suitable for indoors communications and for deployment in small city network, because of the high propagation path loss.

Many studies have investigated the propagation for mm-wave bands in different indoor and outdoor environments [20,28–34]. In [35], the propagation measurements were conducted in the 28 GHz and 73 GHz frequency bands in a typical indoor office environment in downtown Brooklyn, New York on the campus of NYU and a large-scale path loss and temporal statistics was obtained. In [30,33,34,36], extensive propagation measurement campaigns were conducted at 6–38 GHz, which measured path loss and delay spread in indoor corridors and dining rooms. Obtaining this information is vital for the design and operation of future 5G cellular networks that use the mm-wave spectrum. Few studies have made comparison between the frequency band below and above 6 GHz. Three candidate large-scale propagation pathloss models for use over the entire microwave and mm-wave radio spectrum were presented and compared in [37], while a comparative study of the two bands at 2.9 GHz and 29 GHz was provided in [38]. The motivation behind propagation measurements with varying azimuth and elevation angle parameters, using narrow beam width directional antennas in [35,38], is to produce the omni-directional channel models. In this work, wide beam width directional antennas are used for propagation measurement in a closed space environment, i.e., the corridor. Using the wide beam width directional antenna is capable to cover the entire space of the corridor and provides the similar effect as using the omni-directional antenna. This implies that varying azimuth and elevation is not needed for the considered closed corridor environment. Despite this considerable progress in the 5G channel model, a complete characterization of the mm-wave link for next generation 5G mobile broadband is still needed. Thus, this paper will undertake a comparative study between two different bands below and above 6 GHz.

3. Propagation Channel Model

The CI model can be defined as [39]:

$$P_L^{CI}(f, d)[dB] = P_L(f, d_0) + 10n \log_{10} \left(\frac{d}{d_0} \right) + X_\sigma \quad (1)$$

where $P_L(f, d)$ is the path loss at different frequencies with various Tx-Rx separation distance, n is the path-loss exponent (PLE), $P_L(f, d_0)$ is the path loss in dB at a close-in (CI) distance, d_0 , of 1 m, and X_σ is a zero-mean Gaussian-distributed random variable with standard deviation σ dB (shadowing

effect) [40]. The PLE and minimum standard deviation are derived by minimum mean square error (MMSE) approach [30].

The floating-intercept (FI) path loss model is used in the WINNER II and 3GPP standards [35]. It is based on the floating-intercept (α) and line slope (β) to provide a best minimum error fit of collected path losses as follows:

$$PL^{FI}(d)[dB] = \alpha + 10\beta \log_{10}(d) + \chi_{\sigma}^{FI} \quad (2)$$

where χ_{σ}^{FI} is a zero mean Gaussian shadow fading random variable with standard deviation of σ^{FI} . As in the CI model, the MMSE is used as a best-fit and requires solving for α and β to obtain the σ^{FI} .

To cover a broad range of frequencies and measurements, multi-frequency path loss models are used. The alpha-beta-gamma (ABG) model is utilized for this purpose. The proposed ABG model has 1 m as reference distance and 1 GHz as reference frequency (f_{ref} set to 1 GHz). The ABG model is given as:

$$PL^{ABG}(f, d)[dB] = 10\alpha \log_{10}\left(\frac{d}{d_0}\right) + \beta + 10\gamma \log_{10}\left(\frac{f}{f_{ref}}\right) + \chi_{\sigma}^{ABG} \quad (3)$$

where α and γ are constant coefficients which indicate the effect of frequency and distance on path loss, β is referred to as offset in path loss, f is frequency in GHz and χ_{σ}^{ABG} is a Gaussian random variable with standard deviation of σ^{ABG} . The ABG model is solved by MMSE to minimize σ by concurrently solving for α , β and γ [30].

The close-in free space reference distance path loss model, with frequency dependent path loss exponent (CIF), is a multi-frequency model that employs the same physically motivated free space path loss (FSPL) anchor at 1 m, as that of the CI model. The CIF model is defined as [36]:

$$PL^{CIF}(f, d)[dB] = FSPL(f, d_{ref}) + 10n \left(1 + b \left(\frac{f - f_0}{f_0}\right)\right) \log_{10}(d) + \chi_{\sigma}^{CIF}, \quad (4)$$

where n denotes the distance dependence of path loss, and b is a linear frequency dependence factor of path loss over all considered frequencies. The parameter f_0 is the reference frequency, which is the weighted frequency average of all measurements for each specific environment scenario, found by summing up, over all frequencies, the number of measurements at a particular frequency and scenario, multiplied by the corresponding frequency, and dividing that sum by the entire number of measurements taken over all frequencies for that specific environment and scenario [35]. Based on the environment and scenario and the number of measurements at a particular frequency in this work, $f_0 = 10.5$ GHz. The PLE and minimum standard deviation are derived by minimum mean square error (MMSE) [13].

The DL presents the diffraction loss from shadow edge and the FD presents the signal drop for high frequency band as compared with low band.

The DL can be calculated by:

$$DL(f, d)[dB] = \Pr_{LOS}(f, d_0) - \Pr_{NLOS}(f, d_0) \quad (5)$$

where the \Pr_{LOS} represent the received power in LOS scenario and \Pr_{NLOS} is the received power in NLOS scenario.

The FD can be defined as:

$$FD(d)[dB] = \Pr(f < 6GHz, d) - \Pr(f > 6GHz, d) \quad (6)$$

where the $\Pr(f < 6GHz, d)$ is the received power at lower band which is 3.5 GHz in this work and the $\Pr(f > 6GHz, d)$ is the received power at higher band which is 28 GHz in this study.

4. Time Dispersion Parameters

The path loss is the main parameter that can be used to describe the large-scale effects of the propagation channel on the received signal. The RMS delay spread is the main parameter for wideband channel characterization, as it is a good measure of multipath time dispersion. Based on the signal bandwidth, the RMS delay spread provides a good knowledge of the potential severity of inter symbol interference (ISI). The time dispersion characteristics, and analysis of such properties can serve for the indoor mm-wave communications systems design.

The RMS delay spread is defined as the square root of the second moment of a power delay profile (PDP):

$$\tau_{rms} = \sqrt{\overline{\tau^2} - (\overline{\tau_m})^2} \quad (7)$$

where $\overline{\tau^2}$ is the second moment of the PDP and it is given as:

$$\overline{\tau^2} = \frac{\sum_k p(\tau_k) \cdot (\tau_k)^2}{\sum_k p(\tau_k)} \quad (8)$$

and $\overline{\tau_m}$ is the mean excess delay, also given as:

$$\overline{\tau_m} = \frac{\sum_k p(\tau_k) \cdot \tau_k}{\sum_k p(\tau_k)} \quad (9)$$

where p and τ are defined as the power and delay of the k^{th} path, respectively.

5. Experimental Setup

The wideband measurements were conducted using channel sounder equipment as shown in Figure 1. The arbitrary waveform generator (AWG) M8190 (Keysight Technologies, Santa Rosa, CA, USA) was used to generate wideband differential baseband in-phase quadrature (IQ) at the transmitter; it could also output direct intermediate frequency (IF) signals with channel sounding. The baseband arbitrary waveform signal provided 1 ns multipath resolution from a pseudo random binary sequence (PRBS). At the receiver, 12-bit high-speed digitizer (bandwidth = 1 GHz) was used at the receiver for signal acquisition. Details of the measurement equipment can be found in [30]. The measurements were conducted at two different frequencies 3.5 GHz and 28 GHz, along a corridor on the 15th floor of the Menara Tun Razak Building on the Universiti Teknologi Malaysia Kuala Lumpur campus. For LOS scenario, the Tx azimuth (Az) /elevation (El) angles are $0^\circ/0^\circ$ and the Rx azimuth (Az)/elevation (El) angles are $0^\circ/0^\circ$. For NLOS scenario, to cover the edge-wall diffraction, the Tx azimuth (Az)/elevation (El) angles are $45^\circ/0^\circ$ and the Rx azimuth (Az) elevation (El) angles are $0^\circ/0^\circ$.

The measurements have been conducted in the corridor with a size of 2.4 m × 20 m, and the ceiling height is 2.8 m. It has plywood doors, and the walls are constructed of gypsum board and glass. The floor is covered with glazed ceramic tiles, and the corridor ceiling is made of fiberglass materials. A pictorial view of the measurement set up and environment is shown in Figure 2.

To collect all multipath components (MPCs) above the threshold (20 dB below the strongest MPC) [41] from all objects in the corridor, the horn antennas with high gains and wide beamwidths were used in this scenario. Wideband horn antenna (2–24.5 GHz, AINFO Inc., Irvine, CA, USA) was used for Tx and Rx at 3.5 GHz band. The antenna gain is 9 dB and the half power beamwidth (HPBW) values are 58.97° and 61.42° for elevation plane (E-plane) and azimuth plane (H-plane), respectively. At 28 GHz band, a wideband horn antenna (10–40 GHz, ETS-Lindgren Inc., Cedar Park, TX, USA) was used with gain of 11.6 dB and the HPBW values are 44.8° and 37.6° for E-plane and H-plane, respectively for Tx and Rx. At Rx side, a wideband low noise amplifier (LNA, 18–40 GHz, ETS-Lindgren Inc., Cedar Park, TX, USA) was used with gain of 40.3 dB. The wider beamwidth horn antennas have been used that can collect received signal from all objects (i.e., walls, doors and windows

for azimuth plane and ceiling and floor for elevation plane), instead of using narrow beamwidth horn antennas with HPBW below 10° and different azimuth and elevation angles.



Figure 1. Measurement Equipment.



Figure 2. Measurement Environment.

The measurement parameters set up are listed in Table 1. Two scenarios of measurement were carried out along the corridor, LOS and NLOS as shown in Figure 3. For both scenarios, the transmitter (Tx) sets were fixed, while the receiver (Rx) sets were moved along the corridor and the received waveforms were recorded at each 1 m up to the maximum Tx-Rx separation distance, which was 20 m. For the NLOS scenario, the Rx antenna was blocked by the edge of the wall as shown in Figure 3. Here, in this scenario the diffraction phenomena due to the edge shadow has been investigated.

Table 1. Measurement Parameters.

Parameter	Value	Value
Carrier Frequency (GHz)	3.5	28
Transmit Power	0 dBm	0 dBm
Polarization	Vertical	Vertical
Antenna Gain (dB)	9	11.6
Tx and Rx Antenna /HPBW (degree)	58.97	44.8
Tx /Rx Antenna Height (m)	1.5/1.5	1.5/1.5

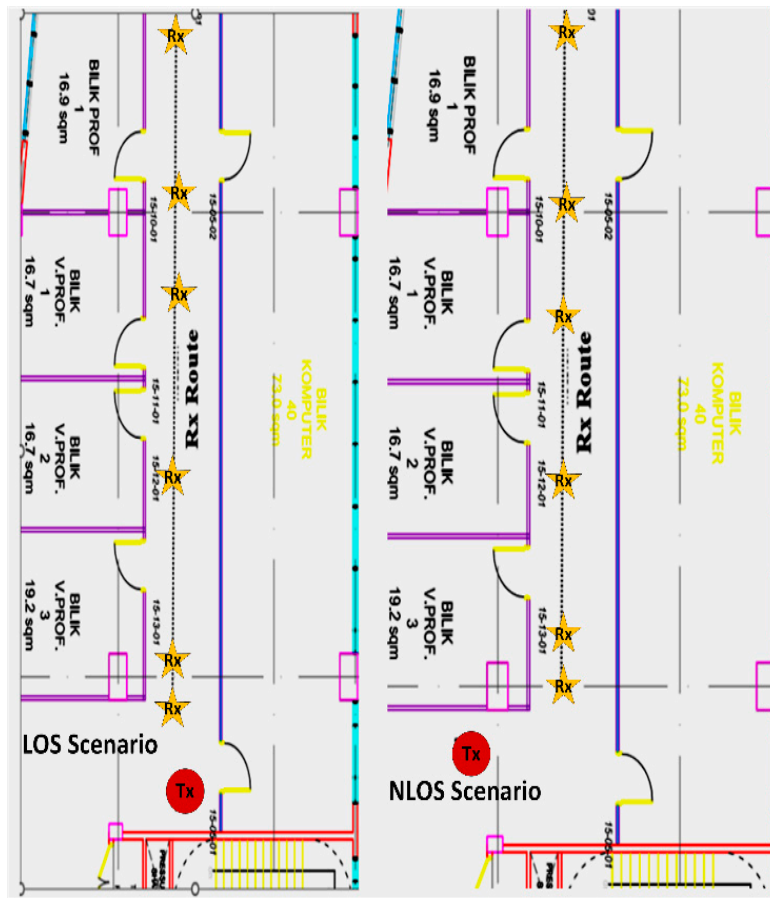


Figure 3. Floor Plan for Measurement Environment.

6. Results and Discussion

As 5G is expected to deliver high amount of data rate, which is useful to design an IoT based smart city network. The use of the mm-wave frequency band in 5G network brings various scattering, fading and penetration losses issues, especially in indoor environment. These issues can be mitigated easily if we can predict the propagation channel, where the signal is propagating. Path loss is one of the important elements to define any channel behavior used for wireless communication. It can depend on many transmission factors, for example, transmitter power, antenna type and its gain, channel structure and its reflection, refraction and diffraction effect. The purpose of path loss modeling is to evaluate the magnitude of attenuation experienced by broadcasting radio signals over a distance, which is useful for designing for 5G communications systems [14]. This section provides the results and analysis for path loss, diffraction, frequency drop, power delay profile and time dispersion parameters. To make an appropriate comparative study for the two measured frequencies, 3.5 GHz (below 6 GHz) and 28 GHz (above 6 GHz), the results of the parameters for both bands are explored in the same figure in each analysis.

6.1. Path Loss Results and Analysis

Figure 4 shows the CI and FI scatter plots and path loss models at 3.5 GHz and 28 GHz for the LOS scenario. Generally, it can be shown that the path loss increases as the distance is increased for both frequencies measured. Using CI models, the path loss exponent (PLE) values are $n = 1.6$ and $n = 1.3$ for 3.5 GHz and 28 GHz, respectively. It is noted that both PLEs are less than the free space path loss exponent $n = 2$ even though the environment is LOS. This implies that the test bed of measurement (indoor corridor) acts as a waveguide; the many reflected signals reach the receiver from both walls on either side, floor and ceiling are added up constructively. From this study as well as many previous

studies in an indoor environment, it is noted that the PLE is not frequency dependent but is strongly environment dependent [30,35]. The standard deviation values of the CI path loss models are 3.2 dB and 1.3 dB for 3.5 GHz and 28 GHz, respectively.

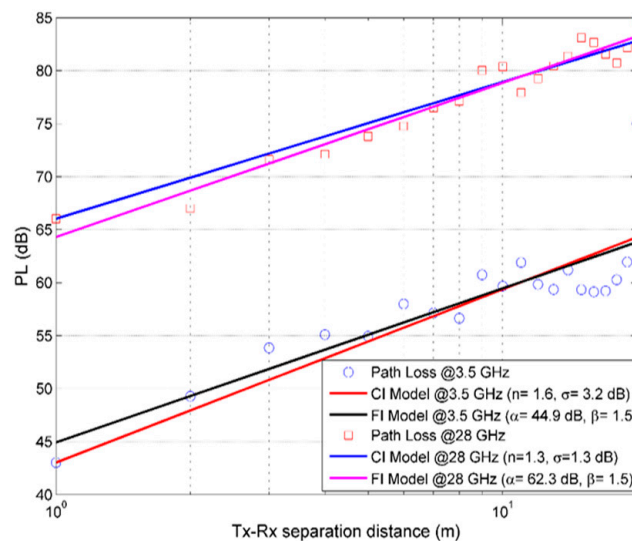


Figure 4. Path loss CI and FI models fitting versus Tx-Rx separation distance at 3.5 GHz and 28 GHz for LOS scenario.

The 3GPP WINNER II model (FI) was also used to investigate the measured data. Figure 4 shows that the FI model also fits the measured data very well at both frequencies. The slope is 1.5 for both bands, which is comparable to the PLE for the CI model. Moreover, the values of the floating intercept (α_{FI}) indicate the validity of this model in bands below and above 6 GHz. The α_{FI} values are 44.9 dB and 62.3 dB for 3.5 GHz and 28 GHz, respectively. These values are slightly different by 1 dB as compared to the free space path loss at reference point of CI model ($d_0 = 1$ m). The standard deviation values for the FI model are 3.0 dB and 1.0 dB for 3.5 GHz and 28 GHz, respectively. The scatter plots of path loss, CI and FI path loss models for the NLOS scenario are shown in Figure 5. From the CI model, it can be shown that the PLE is more than the FSPL exponent for both bands. The PLE values are 2.7 and 3.6 for 3.5 GHz and 28 GHz, respectively. This implies that the signal power drops at a rate of 7 dB/decade and 16 dB/decade more than the signal power drop in the FSPL model (20 dB/decade). For the FI model, the slope (β_{FI}) values are 2.1 and 3; and the α_{FI} values are 48.9 dB and 72.2 dB for 3.5 GHz and 28 GHz, respectively. It is shown from the observed parameters for both the CI and FI models that the signal degradation with Tx-Rx separation distance is more in the 28 GHz band. The α_{FI} values for the FI model deviate from the FSPL at 1 m by 5.6 dB and 10.8 dB for 3.5 GHz and 28 GHz, respectively. Since this model is not physically based, while the CI is physically based, the more accurate parameter for signal drop is the PLE (n).

For multi frequencies, the ABG and CIF path loss models are used to investigate the channel propagation at two different bands; one below 6 GHz (3.5 GHz) and the other is above 6 GHz (28 GHz). The ABG multi-frequency path loss model for the LOS scenario is shown in Figure 6. The distance dependent factor (α_{ABG}) is 1.5 and the frequency dependent factor is ($\gamma = 2.1$). The optimization factor (α_{ABG}) is 33.2 dB. The physical-based multi-frequency path loss model (CIF) is shown in Figure 7. With the fixed reference frequency f_0 of 10.5 GHz, the PLE (n_{CIF}) frequency is 1.5 with the slope of linear frequency dependency ($b = -0.2$). The observed parameters of this model indicate that this model is accurate and simple and is physically-based. For LOS scenario, it can be shown that the both α_{ABG} and n_{CIF} are identical for the ABG and CIF path loss models. This implies that in these measurements the ABG model has good performance for path loss in LOS scenario, although it is not a physically-based model.

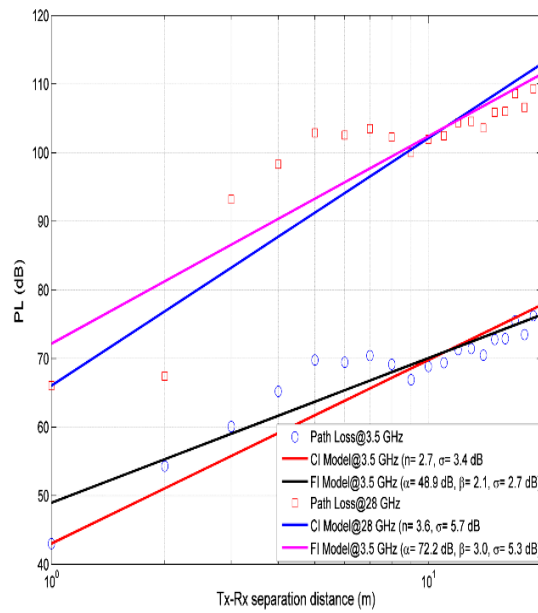


Figure 5. Path loss CI and FI models fitting versus Tx-Rx separation distance at 3.5 GHz and 28 GHz for NLOS scenario.

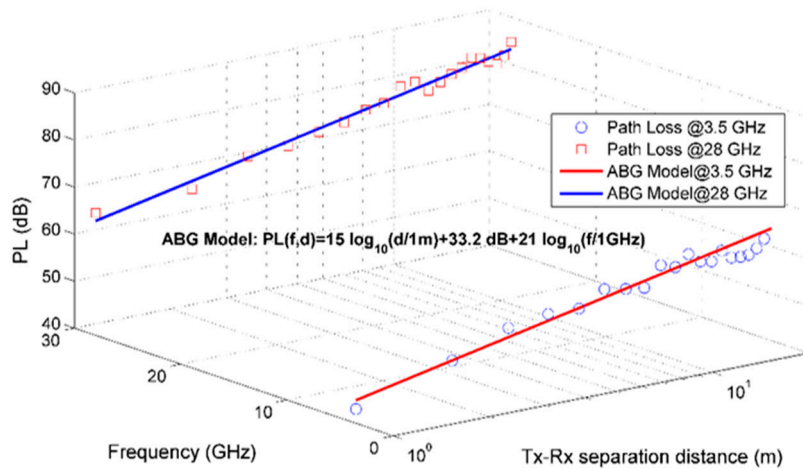


Figure 6. ABG path loss model versus Tx-Rx separation distance for LOS scenario.

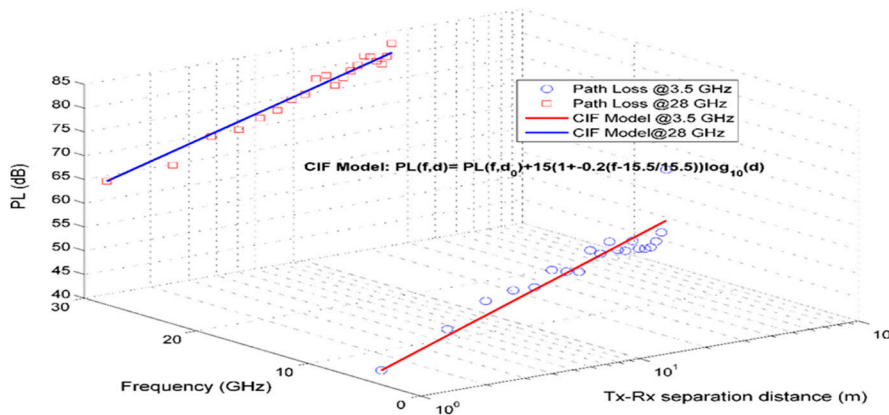


Figure 7. CIF path loss model versus Tx-Rx separation distance for LOS scenario.

Figure 8 shows the ABG path loss model for the NLOS scenario. It can be shown that the ABG model has good fitting for measured data in both bands. The α_{ABG} and γ values are 2.6 and 2.1,

respectively with optimization parameter β_{ABG} of 36.7 dB. The CIF path loss model for the NLOS scenario is shown in Figure 9. The n_{CIF} is 3.1 dB and b is 0.2.

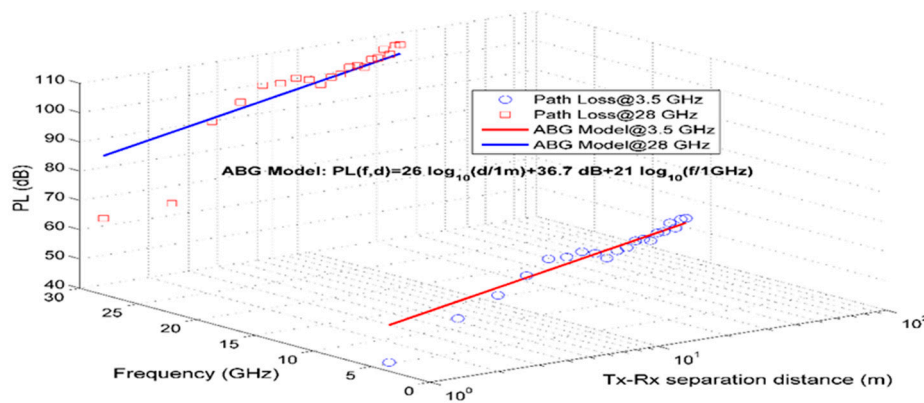


Figure 8. ABG path loss model versus Tx-Rx separation distance for NLOS scenario.

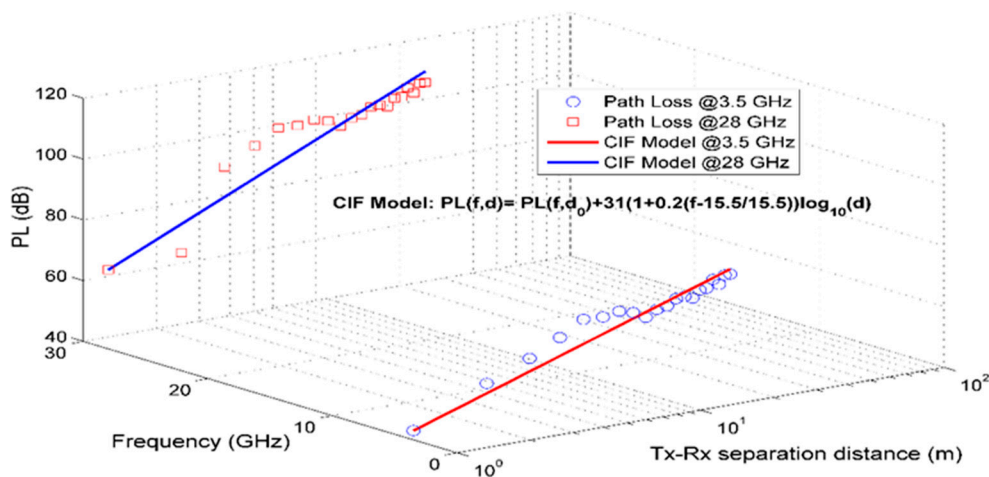


Figure 9. CIF path loss model versus Tx-Rx separation distance for NLOS scenario.

As can be seen from Figure 3 showing how these measurements were obtained, the wall edge blocked the directed paths, hence, these measurements presented a NLOS scenario. The signal degradation in a NLOS scenario represents the diffraction loss (DL). Figure 10 shows the DL and FD values. It presents the power of the received signal (path gain) with Tx-Rx separation distance for LOS and NLOS scenarios at all measured frequencies. The loss due to the shadowing of wall edge (diffraction loss) and the loss due to using a high band above 6 GHz (frequency drop FD) compared to the lower band below 6 GHz are also depicted in Figure 10.

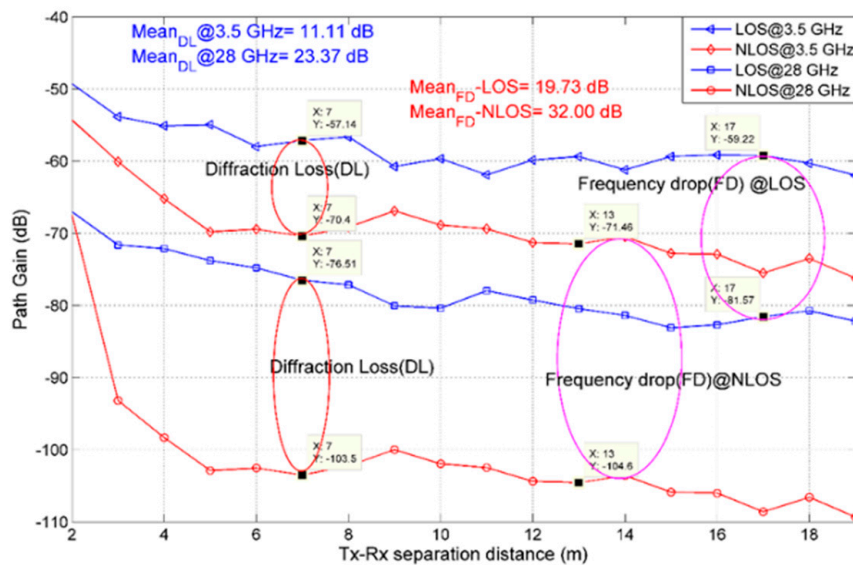


Figure 10. Diffraction loss (DL) and frequency drop (FD) using path gain at different Tx-Rx separation distance.

Figure 10 shows that at 3.5 GHz the path gain at 7 m Tx-Rx separation distance for LOS scenario is -57.14 dB, while, at the NLOS scenario in the same band the path gain is -70.4 dB. This means that for NLOS, the signal degrades by 13.26 dB due to the wall edge shadow that represented the DL proposed parameter. At the same Tx-Rx separation distance of 7 m for 28 GHz, it can be shown that the signal in the NLOS scenario degrades by 27 dB, which is about double of the DL at 3.5 GHz. The means of DL values are 11.11 dB and 23.37 dB for 3.5 GHz and 28 GHz, respectively. It can be concluded that the DL for 28 GHz is high compared to the band below 6 GHz; it is about twice the DL of 3.5 GHz. Another important observation from Figure 10 is the frequency drop, for the LOS scenario at one particular Tx-Rx separation distance of 17 m, where the path gain values are -59.22 and -81.57 dB for 3.5 GHz and 28 GHz, respectively. This implies that the loss due to the higher frequency (FD of signal) is 22.4 dB. In another observation at 13 m of Tx-Rx separation distance for the NLOS scenario the FD loss is 33.14 dB. The mean FD values are 19.73 dB and 32 dB for LOS and NLOS scenarios respectively. The FD loss of the NLOS scenario is greater than that of the LOS scenario, as a mean value, by 12.27 dB, which can represent the DL in the frequency drop estimation.

6.2. Power Delay Profile and Time Dispersion Results and Analysis

Figure 11a,b show the received power for all multipath components at all measurement positions of 3.5 GHz for LOS and NLOS scenarios. For the LOS scenario shown by Figure 11a, it can be shown that most of the received power is concentrated at the early multipath components in the excess delay of less than 10 ns. The highest received power between -60 dBm to -50 dBm is found on the first paths (LOS path) and this power is degraded after a Tx-Rx separation distance of 5 m as shown in Figure 11a. The received power between -75 dB to -61 dB is concentrated at the first 5 multipath components (MPCs) at a time of less than 5 ns. Most of the MPCs have received power in the range of -80 dBm to -76 dBm with an excess delay between 3 ns to 12 ns. Few paths are available at a time above 15 ns with the received power between -100 dBm to -76 dBm. For the NLOS scenario, Figure 11b shows that the received power between -75 dB to -50 dB is found at the earliest excess delay below 10 ns, while most of the received power is in the range of -90 dBm to -77 dBm with excess delay below 30 ns. Some of these MPCs arrived in the range of excess delay 100 ns to 150 ns at the Tx-Rx separation distance between 14 m to 16 m.

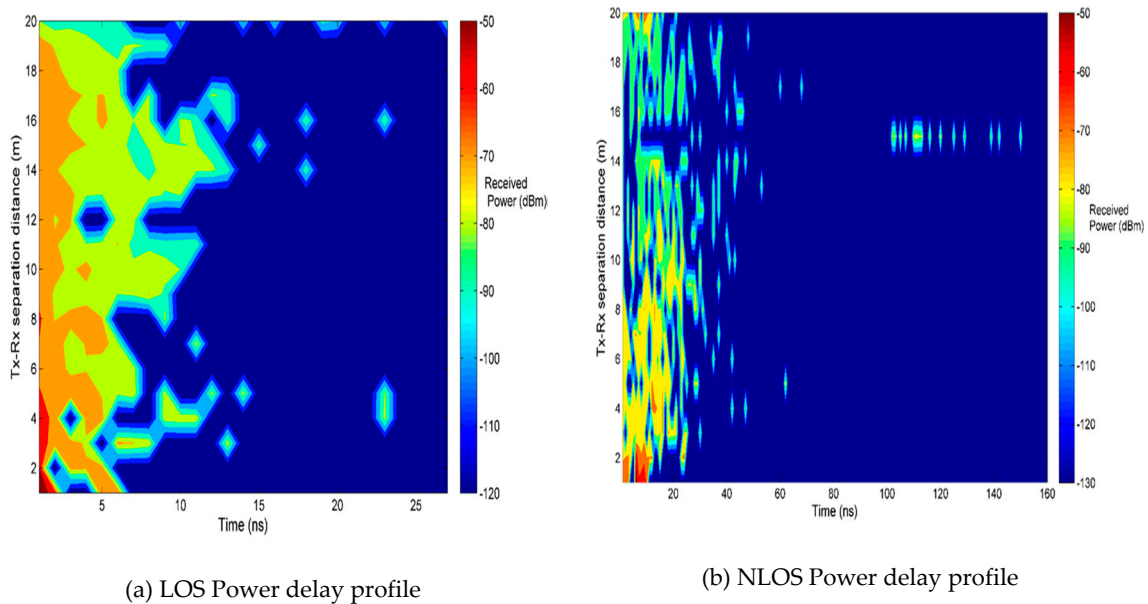


Figure 11. Received power versus time (power delay profile) at all Tx-Rx separation distance in 3.5 GHz band for (a) LOS (b) NLOS.

The received power with excess delay at different Tx-Rx separation distance for 28 GHz is shown in Figure 12a,b for LOS and NLOS scenarios, respectively. Figure 12a shows that the highest received power for the LOS scenario in the 28 GHz band is between -75 dB to -70 dBm in the first 5 m Tx-Rx separation distance with excess delay less than 3 ns.

Some MPCs with less than 4 ns time delay have received power in the range of -80 dBm to -76 dBm. Most of MPCs are ignored after excess delay of 5 ns. For the NLOS scenario, most of MPCs received power less than -100 dBm with excess delay less than 25 ns as shown in Figure 12b. A few paths have received power ranging between -90 dBm and -60 dBm.

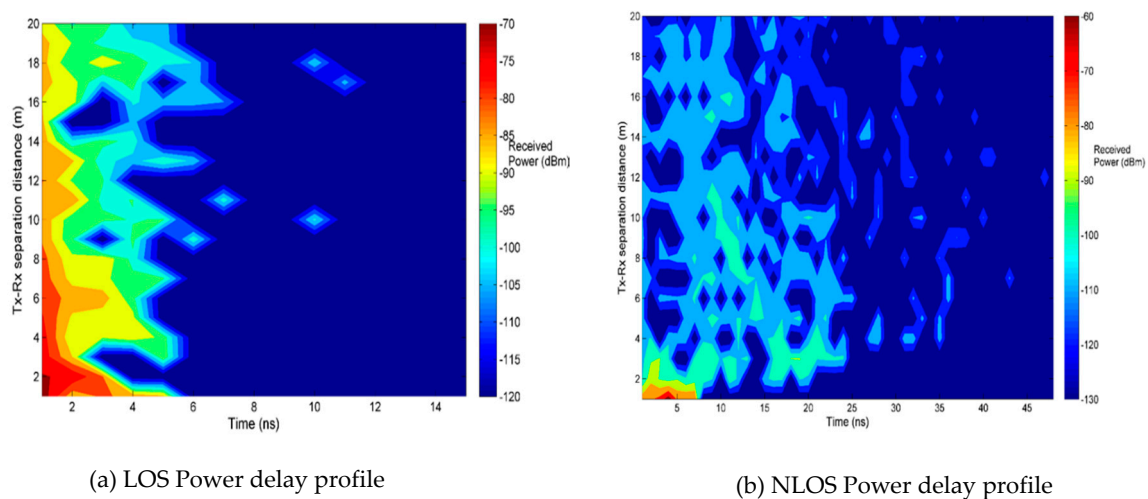


Figure 12. Received power versus time (power delay profile) at all Tx-Rx separation distance in 28 GHz band for (a) LOS (b) NLOS.

Figure 13a,b shows the PDPs for 3.5 GHz and 28 GHz bands in LOS and NLOS scenarios respectively, at one Tx-Rx separation distance of 10 m. Figure 13a, shows the observed MPCs and maximum excess delay for 3.5 GHz and 28 GHz at one pointing angle (the azimuth angle is 0° at the Tx and 60° at the Rx antennas, and the elevation angle is tilted down at the Rx by 5° ; it is 0° at the Tx) for the LOS scenario. In this LOS scenario, it can be shown that using the wide beam horn antenna

although the Rx azimuth was shifted 60° from the Tx angle of 0° and the Rx elevation angle was down tilted 5° from the Tx angle of 0° , the directed path (LOS path) remains the first MPC with maximum power in both bands. The maximum excess are 12 ns and 9 ns for 3.5 GHz and 28 GHz, respectively. For NLOS scenario, Figure 13b, shows the observed MPCs and maximum excess delay for 3.5 GHz and 28 GHz at one pointing angle (the azimuth angle is 45° at the Tx and 60° at the Rx antennas, and the elevation angle is tilted down at the Rx by 5° ; it is 0° at the Tx). Figure 13b shows the strongest path is not the first one for both frequencies because no directed path in NLOS scenario, and the maximum excess delay are more than the excess delay of LOS scenario by 32 ns for both frequencies.

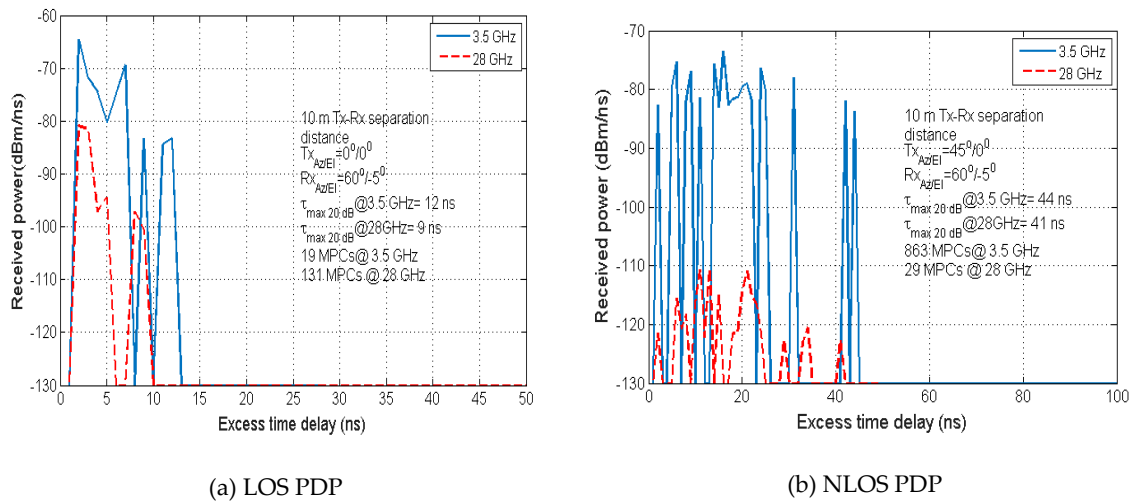


Figure 13. Power delay profiles measured at 3.5 and 28 GHz for a Tx-Rx separation distance of 10 m (a) LOS (b) NLOS.

The RMS delay spread versus Tx-Rx separation distance in both bands for LOS scenario is shown in Figure 14a. The RMS delay spread values for both frequencies are low. The RMS delay spread is less than 4 ns at 3.5 GHz; only at the farthest measurement point is the value of the RMS 7.8 ns.

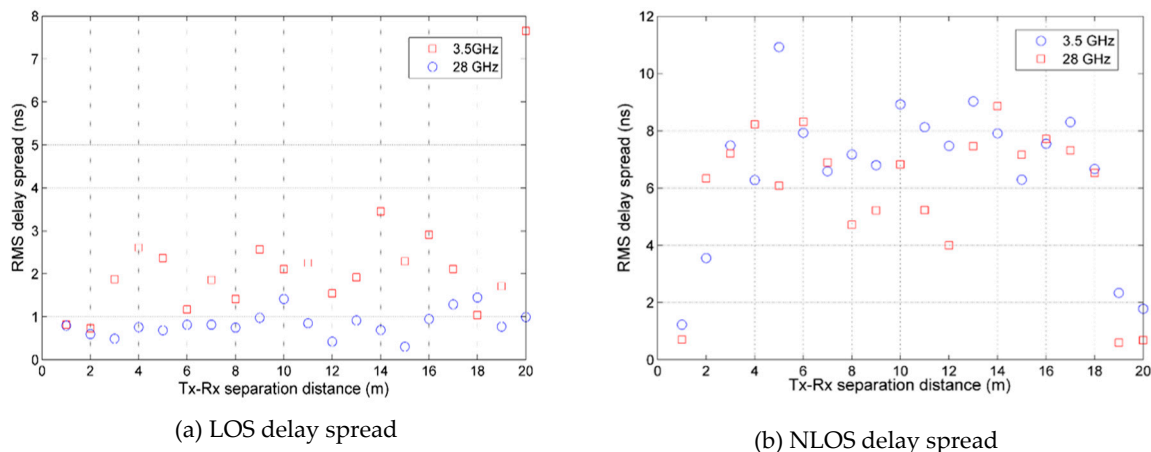


Figure 14. RMS delay spread in both bands 3.5 GHz and 28 GHz for (a) LOS (b) NLOS.

At 28 GHz, the RMS delay spread is less than 2 ns. This indicates that the RMS delay spread is low for the 5G system when the high directive antennas are used at Tx and Rx. This implies that a high data rate can be sent through the 5G channel with less inter symbol interference (ISI). Figure 14b shows the RMS delay spread for the NLOS scenario.

It can be observed that both bands have low RMS delay spread. Moreover, the delay spreads for both frequencies are closer to each other. This indicates that, with the high frequency, the RMS delay

spread does not have any potential change, which encourages the use of the current 3GPP channel model for 5G system with simple modifications in some parameters.

7. Conclusions

This paper has presented the comparative propagation characteristics for the 5G channel at two different frequency bands. Two models have been proposed to study the loss due to the diffraction from wall edge and the loss of high frequency band. The wideband measurements were conducted at 3.5 GHz and 28 GHz using a 5G channel sounder with a high chip rate of 1000 Mcps. The 5G channel parameters for path loss, excess delay and power delay profile were calculated. The signal loss due to the edge shadow and high frequency was investigated. The path loss exponent values for the LOS scenario were 1.6 and 1.3 at 3.5 and 28 GHz, respectively. However, the received power was dropped in the NLOS scenario, where the PLE values were 2.7 and 3.6 at 3.5 GHz and 28 GHz, respectively. The 3GPP models i.e., FI and ABG provided reliable performance for path loss for both single and multi-frequency models in LOS scenario. Based on the proposed models, the average diffraction loss values were 11.11 dB and 23.37 dB at 3.5 GHz and 28 GHz respectively. The loss due to frequency, termed frequency drop was 19.73 dB for the LOS scenario and 32.00 for the NLOS scenario. The RMS delay spread values were less than 8 ns and 12 ns at both frequency bands, for the LOS and NLOS scenarios, respectively. These results indicate that the 5G channel has good performance in term of path loss with very low delay spread. The findings in this study are useful to test and implement for real environment and gives a sight for the next-generation IoT based smart city 5G network. This also implies that the future 5G wireless networks can support a high data rate with low latency using high directive antenna to provide high gain power with small cell size.

Author Contributions: Conceptualization, A.M.A.-S., T.A.R. and T.A.-H.; methodology, A.M.A.-S., T.A.R. and T.A.-H.; A.D., and M.N.H.; software validation, A.M.A.-S., T.A.R., T.A.-H., A.D., M.N.H., M.H.A., K.D. and M.A.; formal analysis, A.M.A.-S., T.A.R. and T.A.-H.; investigation, A.M.A.-S., T.A.R. and T.A.-H.; resources A.M.A.-S., T.A.R. and T.A.-H.; data curation, A.M.A.-S., T.A.R., T.A.-H., A.D. and M.N.H.; writing—original draft preparation, A.M.A.-S.; writing—review and editing, A.M.A.-S., T.A.R., T.A.-H., A.D., M.N.H., M.H.Z., K.D. and M.A.; visualization, A.M.A.-S., T.A.R. and T.A.-H.; supervision, T.A.R.; project administration, A.M.A.-S., T.A.R. and T.A.-H.; funding acquisition, T.A.R. and T.A.-H.

Funding: This research was funded by Research Management Centre (RMC), Universiti Teknologi Malaysia (UTM) and School of Science and Technology, Nottingham Trent University.

Acknowledgments: We would like to thank the Research Management Centre (RMC) at Universiti Teknologi Malaysia(UTM) for funding this work (Vot 04E21) jointly with the NICS group at Nottingham Trent University, Nottingham, United Kingdom.

Conflicts of Interest: The authors declare no conflict of interest.

References

1. Ofcom. Spectrum above 6 GHz for Future Mobile Communications. Available online: https://www.ofcom.org.uk/_data/assets/pdf_file/0023/69422/spectrum_above_6_ghz_cfi.pdf (accessed on 16 January 2015).
2. Vasjanov, A.; Barzdenas, V. A Review of Advanced CMOS RF Power Amplifier Architecture Trends for Low Power 5G Wireless Networks. *Electronics* **2018**, *7*, 271. [[CrossRef](#)]
3. Qamar, F.; Dimyati, K.B.; Hindia, M.N.; Noordin, K.A.B.; Al-Samman, A.M. A comprehensive review on coordinated multi-point operation for LTE-A. *Comput. Netw.* **2017**, *123*, 19–37. [[CrossRef](#)]
4. Member, D.H.; Ai, B.; Member, S.; Member, K.G.; Student, L.W. The Design and Applications of High-Performance Ray-Tracing Simulation Platform for 5G and Beyond Wireless Communications: A Tutorial. *IEEE Commun. Surv. Tutor.* **2018**, 1–18. [[CrossRef](#)]
5. Cero, E.; Baraković Husić, J.; Baraković, S. IoT's Tiny Steps towards 5G: Telco's Perspective. *Symmetry* **2017**, *9*, 213. [[CrossRef](#)]
6. Chiu, W.; Su, C.; Fan, C.; Chen, C.; Yeh, K.-H. Authentication with What You See and Remember in the Internet of Things. *Symmetry* **2018**, *10*, 537. [[CrossRef](#)]

7. Parada, R.; Cárdenes-Tacoronte, D.; Monzo, C.; Melià-Seguí, J. Internet of Things Area Coverage Analyzer (ITHACA) for Complex Topographical Scenarios. *Symmetry* **2017**, *9*, 237. [CrossRef]
8. Elijah, O.; Rahman, T.A.; Orikumhi, I.; Leow, C.Y.; Hindia, M.N. An Overview of Internet of Things (IoT) and Data Analytics in Agriculture: Benefits and Challenges. *IEEE Internet Things J.* **2018**, *4662*, 1–17. [CrossRef]
9. Al Hadhrami, T.; Wang, Q.; Grecos, C. Power- and Node-Type-Aware Routing Algorithm for Emergency-Response Wireless Mesh Networks. In Proceedings of the IEEE 77th Vehicular Technology Conference (VTC Spring), Dresden, Germany, 2–5 June 2013; pp. 1–5.
10. Syafrudin, M.; Alfian, G.; Fitriyani, N.; Rhee, J. Performance Analysis of IoT-Based Sensor, Big Data Processing, and Machine Learning Model for Real-Time Monitoring System in Automotive Manufacturing. *Sensors* **2018**, *18*, 2946. [CrossRef]
11. Akdeniz, M.R.; Liu, Y.; Samimi, M.K.; Sun, S.; Rangan, S.; Rappaport, T.S.; Erkip, E. Millimeter Wave Channel Modeling and Cellular Capacity Evaluation. *IEEE J. Sel. Areas Commun.* **2014**, *32*, 1164–1179. [CrossRef]
12. Andrews, J.G.; Buzzi, S.; Choi, W.; Hanly, S.V.; Lozano, A.; Soong, A.C.K.; Zhang, J.C. What Will 5G Be? *IEEE J. Sel. Areas Commun.* **2014**, *32*, 1065–1082. [CrossRef]
13. ITU. The Technical Feasibility of IMT in the Bands above 6 GHz. Available online: <https://www.itu.int/pub/R-REP-M.2376> (accessed on 2 February 2015).
14. Wang, C.; Bian, J.; Sun, J.; Zhang, W. A Survey of 5G Channel Measurements and Models. *IEEE Commun. Surv. Tutor.* **2018**, *20*, 3142–3168. [CrossRef]
15. Rappaport, T.S.; Xing, Y.; Member, S.; Maccartney, G.R.; Member, S.; Molisch, A.F. Overview of Millimeter Wave Communications for a Focus on Propagation Models. *IEEE Trans. Antennas Propag.* **2017**, *65*, 6213–6230. [CrossRef]
16. Mezzavilla, M.; Polese, M.; Zanella, A.; Dhananjay, A.; Rangan, S.; Kessler, C.; Rappaport, T.S.; Zorzi, M. Public Safety Communications above 6 GHz: Challenges and Opportunities. *IEEE Access* **2018**, *6*, 316–329. [CrossRef]
17. Kaya, A.O.; Calin, D.; Viswanathan, H. 28 GHz and 3.5 GHz Wireless Channels: Fading, Delay and Angular Dispersion. In Proceedings of the IEEE Global Communications Conference (GLOBECOM), Washington, DC, USA, 4–8 December 2016; pp. 1–7.
18. Testbed, N.R.; Coverage, G.; Halvarsson, B.; Simonsson, A.; Elgcróna, A.; Chana, R.; Machado, P.; Asplund, H. 5G NR Testbed 3.5 GHz Coverage Results. In Proceedings of the 2018 IEEE 87th Vehicular Technology Conference, Porto, Portugal, 3–6 June 2018; pp. 2–6. [CrossRef]
19. Xiao, M.; Mumtaz, S.; Huang, Y.; Dai, L.; Li, Y.; Matthaiou, M.; Karagiannidis, G.K.; Bjornson, E.; Yang, K.; Chih-Lin, I.; Ghosh, A. Millimeter Wave Communications for Future Mobile Networks. *IEEE J. Sel. Areas Commun.* **2017**, *35*, 1909–1935. [CrossRef]
20. Rappaport, T.S.; MacCartney, G.R.; Samimi, M.K.; Sun, S. Wideband Millimeter-Wave Propagation Measurements and Channel Models for Future Wireless Communication System Design. *IEEE Trans. Commun.* **2015**, *63*, 3029–3056. [CrossRef]
21. Andrisano, O.; Tralli, V.; Verdone, R. Millimeter waves for short-range multimedia communication systems. *Proc. IEEE* **1998**, *86*, 1383–1401. [CrossRef]
22. Voigtlander, F.; Ramadan, A.; Eichinger, J.; Lenz, C.; Pensky, D.; Knoll, A. 5G for robotics: Ultra-low latency control of distributed robotic systems. In Proceedings of the 2017 International Symposium on Computer Science and Intelligent Controls (ISCSIC), Budapest, Hungary, 20–22 October 2017; pp. 69–72. [CrossRef]
23. Sachs, J.; Andersson, L.A.A.; Araujo, J.; Curescu, C.; Lundsjo, J.; Rune, G.; Steinbach, E.; Wikstrom, G. Adaptive 5G Low-Latency Communication for Tactile Internet Services. *Proc. IEEE* **2018**, *99*, 1–25. [CrossRef]
24. Pandit, S.; Fitzek, F.H.P.; Redana, S. Demonstration of 5G connected cars. In Proceedings of the 2017 14th IEEE Annual Consumer Communications & Networking Conference (CCNC), Las Vegas, NV, USA, 8–11 January 2017; pp. 605–606.
25. Pandi, S.; Fitzek, F.H.P.; Lehmann, C.; Nophut, D.; Kiss, D.; Kovacs, V.; Nagy, A.; Csorvasi, G.; Toth, M.; Rajacsis, T.; et al. Joint Design of Communication and Control for Connected Cars in 5G Communication Systems. In Proceedings of the 2016 IEEE Globecom Workshops (GC Wkshps), Washington, DC, USA, 4–8 December 2016; pp. 1–7.
26. Abbas, T.; Qamar, F.; Ahmed, I.; Dimiyati, K.; Majed, M.B. Propagation channel characterization for 28 and 73 GHz millimeter-wave 5G frequency band. In Proceedings of the 2017 IEEE 15th Student Conference on Research and Development (SCoReD), Putrajaya, Malaysia, 13–14 December 2017; pp. 297–302.

27. Niu, Y.; Li, Y.; Jin, D.; Su, L.; Vasilakos, A.V. A survey of millimeter wave communications (mmWave) for 5G: Opportunities and challenges. *Wirel. Netw.* **2015**, *21*, 2657–2676. [[CrossRef](#)]
28. Wang, Q.; Li, S.; Zhao, X.; Wang, M.; Sun, S. Wideband Millimeter-Wave Channel Characterization Based on LOS Measurements in an Open Office at 26 GHz. In Proceedings of the 2016 IEEE 83rd Vehicular Technology Conference (VTC Spring), Nanjing, China, 15–18 May 2016; pp. 1–5.
29. Hur, S.; Cho, Y.-J.; Lee, J.; Kang, N.-G.; Park, J.; Benn, H. Synchronous channel sounder using horn antenna and indoor measurements on 28 GHz. In Proceedings of the 2014 IEEE International Black Sea Conference on Communications and Networking (BlackSeaCom), Odessa, Ukraine, 27–30 May 2014; pp. 83–87.
30. Al-Samman, A.M.; Rahman, T.A.; Azmi, M.H.; Hindia, M.N.; Khan, I.; Hanafi, E. Statistical Modelling and Characterization of Experimental mm-Wave Indoor Channels for Future 5G Wireless Communication Networks. *PLoS ONE* **2016**, *11*, e0163034. [[CrossRef](#)]
31. Azar, Y.; Wong, G.N.; Wang, K.; Mayzus, R.; Schulz, J.K.; Zhao, H.; Gutierrez, F.; Hwang, D.; Rappaport, T.S. 28 GHz propagation measurements for outdoor cellular communications using steerable beam antennas in New York city. In Proceedings of the 2013 IEEE International Conference on Communications (ICC), Budapest, Hungary, 9–13 June 2013; pp. 5143–5147.
32. MacCartney, G.R.; Zhang, J.; Nie, S.; Rappaport, T.S. Path loss models for 5G millimeter wave propagation channels in urban microcells. In Proceedings of the 2013 IEEE Global Communications Conference (GLOBECOM), Atlanta, GA, USA, 9–13 December 2013; pp. 3948–3953.
33. Oyie, N.O.; Member, S.; Afullo, T.J.O. Measurements and Analysis of Large-Scale Path Loss Model at 14 and 22 GHz in Indoor Corridor. *IEEE Access* **2018**, *6*, 17205–17214. [[CrossRef](#)]
34. Al-samman, A.M.; Rahman, T.A.; Azmi, M.H. Millimeter-Wave Propagation Measurements and Models at 28 GHz and 38 GHz in a Dining Room for 5G Wireless Networks. *Measurement* **2018**, *130*, 71–81. [[CrossRef](#)]
35. Maccartney, G.R.; Rappaport, T.S.; Sun, S.; Deng, S. Indoor Office Wideband Millimeter-Wave Propagation Measurements and Channel Models at 28 and 73 GHz for Ultra-Dense 5G Wireless Networks. *IEEE Access* **2015**, *3*, 2388–2424. [[CrossRef](#)]
36. Al-samman, A.M.; Rahman, T.A.; Azmi, M.H. Indoor Corridor Wideband Radio Propagation Measurements and Channel Models for 5G Millimeter Wave Wireless Communications at 19 GHz, 28 GHz, and 38 GHz Bands. *Wirel. Commun. Mob. Comput.* **2018**, *2018*, 1–12. [[CrossRef](#)]
37. Sun, S.; Rappaport, T.S.; Thomas, T.A.; Ghosh, A.; Nguyen, H.C.; Kovacs, I.Z.; Rodriguez, I.; Koymen, O.; Partyka, A. Investigation of Prediction Accuracy, Sensitivity, and Parameter Stability of Large-Scale Propagation Path Loss Models for 5G Wireless Communications. *IEEE Trans. Veh. Technol.* **2016**, *65*, 2843–2860. [[CrossRef](#)]
38. Koymen, O.H.; Partyka, A.; Subramanian, S.; Li, J. Indoor mm-Wave Channel Measurements: Comparative Study of 2.9 GHz and 29 GHz. In Proceedings of the 2015 IEEE Global Communications Conference (GLOBECOM), San Diego, CA, USA, 6–10 December 2015; pp. 1–6.
39. MacCartney, G.R.; Rappaport, T.S. Rural Macrocell Path Loss Models for Millimeter Wave Wireless Communications. *IEEE J. Sel. Areas Commun.* **2017**, *35*, 1663–1677. [[CrossRef](#)]
40. Rappaport, T.S. *Wireless Communications Principles and Practice*, 2nd ed.; Prentice Hall: Upper Saddle River, NJ, USA, 2002.
41. ITU. Multipath Propagation and Parameterization of Its Characteristics. Recommendation ITU-R P.1407-6. Available online: <https://www.itu.int/rec/R-REC-P.1407-6-201706-1/en> (accessed on 20 June 2017).

